



Redox-responsive AIE micelles for intracellular paclitaxel delivery

Qiang Wang¹ · Feng Gao¹ · Xianyong Zhou¹

Received: 22 February 2020 / Revised: 22 April 2020 / Accepted: 25 May 2020
© Springer-Verlag GmbH Germany, part of Springer Nature 2020

Abstract

Compared with conventional drug nanocarriers, multifunctional drug delivery systems exhibited characteristic advantages. In this study, we developed a multifunctional drug delivery system possessing stimuli-responsive drug release and cellular imaging. Amphiphilic polymers, methoxypolyethylene glycol-cystamine-tetraphenylethene (mPEG_{1k}-SS-TPE), were synthesized by combining methoxypolyethylene glycol (mPEG_{1k}) and tetraphenylethene (TPE) using reduction-sensitive disulfide bonds that can be disconnected by high level of inherent glutathione (GSH). Size distribution and morphology of mPEG_{1k}-SS-TPE micelles were evaluated. Meanwhile, the reduction-sensitivity of mPEG_{1k}-SS-TPE micelles was surveyed compared with that of mPEG_{1k}-TPE micelles. Nile Red was encapsulated into mPEG_{1k}-SS-TPE micelles to visually observe intracellular drug delivery against SW480 cells. Paclitaxel (PTX) was chosen to be loaded into micelles to evaluate the cytotoxicity against HCT116, HT-29, and SW480.

Keywords Reduction-sensitive · Cellular imaging · Aggregation-induced emission · Paclitaxel

Introduction

Chemotherapy is one of the most commonly used methods in cancer therapies. Unfortunately, many chemotherapeutic agents often cause severe side effects because of non-specific distribution. To overcome this issue, many nanocarriers, including micelles [1–3], liposomes [4–6], and organic or inorganic nanoparticles [7–10], have been explored to enhance the anticancer activity and reduce the side effects of these chemotherapeutic agents. These nanocarriers can accumulate in tumor tissues during blood circulation based on the enhanced permeation and retention (EPR) effect [11–13].

After the drug delivery systems reach the desired target sites, rapid release of the loaded drugs is required to achieve efficacy. Therefore, it is desirable to construct drug delivery systems with stimuli-responsive release mechanisms. Stimuli-responsiveness of drug delivery systems is often endowed by

introducing stimuli-responsive chemical bonds, like GSH-sensitive disulfide bonds. GSH is a thiol tripeptide that is composed of glutamic acid, cysteine, and glycine, capable of reducing disulfide bonds [1, 14–16]. The tumor intracellular GSH concentration (2–10 mM) is known to be substantially higher than the level in the cellular exterior (2–20 μM) [17–19]. This dramatic variation of the GSH concentration makes it possible to design intracellular GSH-responsive drug release.

Recently, molecules with aggregation-induced emission (AIE) attracted the interest of the researchers [20, 21]. As reported, AIE molecules exhibited strong fluorescence in an aggregated state, but weak fluorescence in a free state [22–24]. It is more interesting when AIE molecules were combined with amphiphilic polymers and used to design DDSs. It has been reported that TPE-mPEG was synthesized by conjugating TPE with mPEG (MW 2000) [25]. After self-assembly in water, TPE-mPEG micelles displayed AIE fluorescence, which can be used to trace intracellular drug delivery.

Inspired by these researches, we combined PEG and TPE with disulfide bonds to generate poly(ethylene glycol) methyl ether-disulfide-tetraphenylethene (mPEG_{1k}-SS-TPE). Poly(ethylene glycol) methyl ether (MW 1000) was selected to provide hydrophilic segments, thus leading to smaller critical micelle concentration (CMC). The hydrophobic TPE moiety was introduced as the hydrophobic moiety to entrap hydrophobic anticancer drugs. TPE, as the typical AIE building

Electronic supplementary material The online version of this article (<https://doi.org/10.1007/s00396-020-04679-4>) contains supplementary material, which is available to authorized users.

✉ Qiang Wang
bzphqiangwang@163.com

¹ Department of General Surgery, Binzhou People's Hospital, Binzhou 256600, China

block, has been widely used for construction of efficient luminescent materials [26–28]. Contrary to traditional chromophores with aggregation-caused quenching (ACQ) effect, TPE shows high emission efficiency when it is aggregated in poor solvents, while weak emission efficiency when it is in good solvents. The switching on or off of AIE micelles dynamically reflects the real-time state and location of intracellular micelles. Besides, TPE exhibited better chemical stability due to its chemical structure and photostability (except for UV irradiation) [25]. On the basis of these properties, TPE was firstly conjugated with cystamine to generate TPE-SS-NH₂. Then, mPEG_{1k}-OH was activated by succinic anhydride to produce mPEG_{1k}-COOH that was further modified with TPE-SS-NH₂ (Scheme 2). The generated mPEG_{1k}-SS-TPE can self-assemble into micelles, which exhibits significant fluorescence (Scheme 1). PTX can be encapsulated into micelles. After entering into tumor cells, PTX-loaded mPEG_{1k}-SS-TPE micelles can be degraded by high level of GSH, and thus PTX can be released to inhibit tumor growth.

Materials and methods

Materials

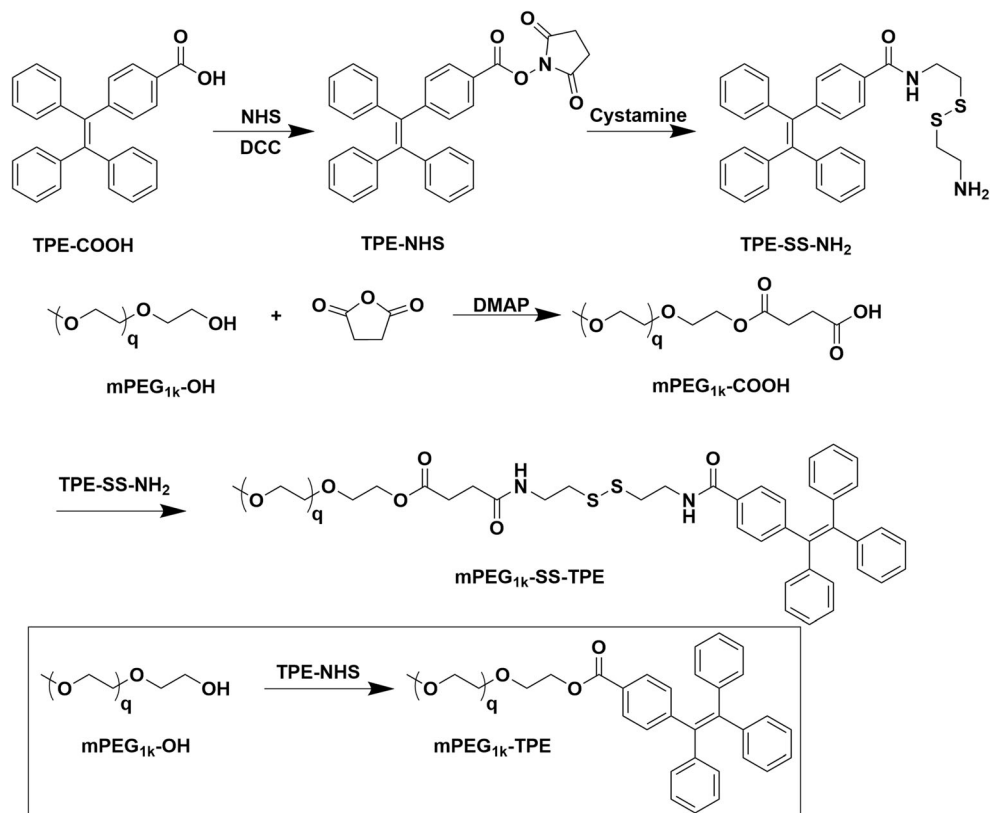
Methoxy polyethylene glycol (mPEG_{1k}-OH, MW 1000 Da) and succinic anhydride were bought from Shanghai

Mclin Biochemical Technology Co., Ltd. Dicyclohexylcarbodiimide (DCC) and *N*-hydroxysuccinimide (NHS) were purchased by Shanghai Aladdin Biochemical Technology Co., Ltd. 4-Dimethylaminopyridine (DMAP) and cystamine dihydrochloride were purchased from Shanghai Meryer Chemical Technology Co., Ltd. 4-(1,2,2-Triphenyl vinyl)benzoic acid (TPE-COOH) was purchased from Energy Chemical. PTX was purchased from Tianjin Shiensi biochemical Technology Co., Ltd. Glutathione (GSH) and glutathione ethyl ester (GSH-OEt) were purchased from Sigma-Aldrich. All solvents including dichloromethane (DCM), tetrahydrofuran (THF), methanol, and chloroform were purchased from General-Reagent and used as received.

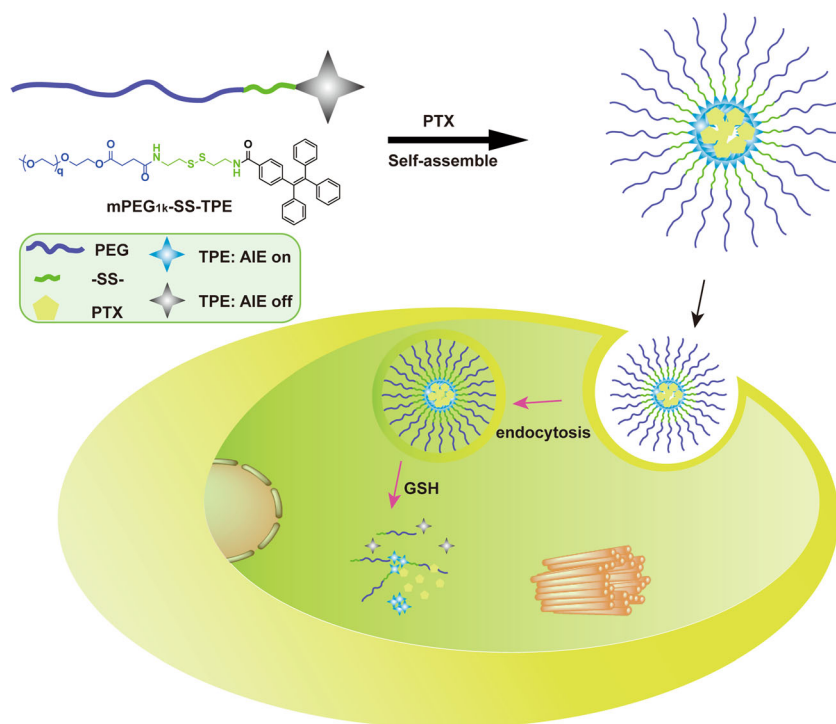
Synthesis of TPE-NHS

TPE-COOH was activated by DCC/NHS method. Briefly, TPE-COOH (1.5 g, 4 mmol) and NHS (0.56 g, 4.8 mmol) were dissolved in 20-mL DCM completely. Then, DCC (1.2 g, 6 mmol) was dissolved in 20-mL DCM and mixed with TPE-COOH/NHS solution. After reaction for 12 h, the reaction mixture was filtrated and washed with saturated NaCl solution. The collected organic phase was dried with anhydrous Na₂SO₄ for 4 h. TPE-NHS was obtained after filtration and concentration as white solid (1.4 g, yield 74.0%).

Scheme 2 Synthetic routes of mPEG_{1k}-SS-TPE



Scheme 1 Preparation of the PTX-loaded mPEG_{1k}-SS-TPE micelles and intracellular release behavior



Synthesis of TPE-SS-NH₂

Before synthesis of TPE-SS-NH₂, cystamine dihydrochloride (1.0 g, 4.4 mmol) was dissolved in 10-mL NaOH solution (1 mM) and the aqueous solution was stirred at room temperature for 4 h. Extraction with DCM was performed twice. After discarding the aqueous phase, organic phase was collected and dried with anhydrous Na₂SO₄. After filtration, cystamine solution was collected and TPE-NHS (1.0 g, 2.1 mmol) in DCM was added slowly. The reaction was stirred at room temperature for another 8 h. TPE-SS-NH₂ was obtained by column chromatography (DCM/methanol 40/1) (0.71 g, yield 66.3%).

Synthesis of mPEG-COOH

Succinic anhydride was used to modify mPEG-OH. In brief, mPEG-OH (5.0 g, 6.7 mmol) and succinic anhydride (1.7 g, 16.7 mmol) were suspended in DCM. The suspension was refluxed at 40 °C. DMAP (0.08 g, 0.7 mmol) was added into the reaction mixture. With the progress of the reaction, succinic anhydride gradually dissolved, and the reaction gradually became clear and yellow. After reaction for 24 h, thin-layer chromatography (TLC) assay exhibited that the reaction was complete. Afterwards, the reaction mixture was cooled and washed with saturated NaCl solution. After evaporation of DCM, the residue was re-dissolved in saturated NaCl solution and stirred at 60 °C for 30 min. After cooling down to room temperature, the aqueous solution was extracted with DCM for 3 times. The collected organic phase was washed

with saturated NaHCO₃ solution and dried with anhydrous Na₂SO₄. The final product was obtained by filtration and concentration as oil liquid (4.8 g, yield 84.3%).

Synthesis of mPEG_{1k}-SS-TPE

mPEG_{1k}-COOH (0.68 g, 0.62 mmol), DCC (0.019 g, 0.93 mmol), and NHS (0.11 g, 0.93 mmol) were dissolved in 15-mL DCM and stirred at room temperature for 4 h. TPE-SS-NH₂ (0.51 g, 1.0 mmol) in 10 mL was added. The reaction was performed for another 12 h. TLC assay showed the reaction was complete. After filtration and extraction with saturated NaCl solution, mPEG_{1k}-SS-TPE was obtained by column chromatography (DCM/methanol 30/1) (0.66 g, yield 66.1%).

To further investigate the properties of mPEG_{1k}-SS-TPE, mPEG_{1k}-TPE was synthesized by conjugation of mPEG_{1k}-OH with TPE-NHS.

Characterization of polymers

The chemical structure of polymers was detected by ¹H NMR on Bruker (500 MHz) in CDCl₃ or DMSO-*d*₆. The critical micelle concentration (CMC) of amphiphilic polymers was determined by a simple method based on AIE effect. Briefly, the solution with different concentration of mPEG_{1k}-SS-TPE or mPEG_{1k}-TPE in methanol was prepared and added into brown vial. After volatilization of methanol, same volume of pure water was added. Then, the solution was processed by ultrasound for 30 min and incubated at 37 °C in the dark for 24 h before fluorescence measurement. The fluorescence

absorbance values at 480 nm were collected to calculate the CMC.

Preparation of micelles

Micelles based on mPEG_{1k}-SS-TPE were prepared by thin-film hydration method. Briefly, mPEG_{1k}-SS-TPE or mPEG_{1k}-TPE was dissolved in DCM and evaporated to form thin film. After being dried under vacuum for 4 h, ultrapure water was added to hydrate at room temperature for 4 h. Micelles were obtained after filtration through 0.45- μ m Millipore filter membrane.

Characterization of micelles

Size distribution and morphology of micelles were demonstrated by dynamic light scattering (DLS) and transmission electron microscopy (TEM), respectively. The stability of micelles was monitored by DLS. The reduction sensitivity of mPEG_{1k}-SS-TPE micelles was determined by DLS and TEM. Photos of mPEG_{1k}-SS-TPE micelles treated with GSH were taken to visually observe the reduction sensitivity.

Drug encapsulation and release

PTX-loaded mPEG_{1k}-SS-TPE micelles (PTX-PSSTMs) were prepared by solvent evaporation method [29]. Briefly, 15-mg PTX and 100-mg mPEG_{1k}-SS-TPE were dissolved in chloroform. Then, the solution was evaporated to form a thin film at 60 °C. PTX-PSSTMs were obtained by hydrating the film with ultrapure water. At last, the solution was filtrated through 0.45- μ m Millipore filter membrane, following dialysis against pure water for 24 h with three times of changing water. As comparison, PTX-loaded mPEG_{1k}-TPE micelles (PTX-PTMs) were prepared by the same method. Nile Red-loaded mPEG_{1k}-SS-TPE and mPEG_{1k}-TPE micelles were prepared with the same method. The drug loading content (DLC) and drug loading efficiency (DLE) were measured according to the report [30], and calculated as follows:

$$\text{DLC}\% = \frac{\text{weight of PTX loaded}}{\text{weight of PTX loaded micelles}} \times 100\% \quad (1)$$

$$\text{DLE}\% = \frac{\text{weight of PTX loaded}}{\text{weight of PTX in feeding}} \times 100\% \quad (2)$$

PTX release in vitro was simulated in phosphate buffer solution (PBS, 0.2 M, pH 7.4) containing 0.1% Tween 80. And different amount of GSH was added to make a final concentration of 20 μ M, 2 mM, or 10 mM GSH. PTX-

loaded micelles were added into dialysis bag (MW 2000) that was sealed and incubated at 37 °C in release medium for 48 h. At predetermined time, 2-mL medium was withdrawn to measure PTX concentration and an equal volume of fresh medium was immediately added.

Cellular uptake

SW480 cells were seeded in 6-well plates (3.0×10^5 cells/well), maintained in 2-mL DMEM with 10% FBS and 50 U/mL penicillin and 50 U/mL streptomycin, and incubated at 37 °C in the atmosphere containing 5% CO₂ for 24 h. After that, the growth medium was replaced with 2-mL medium containing Nile Red-loaded mPEG_{1k}-SS-TPE or mPEG_{1k}-TPE micelles. After further incubation for 0.5 h, 1 h, and 2 h, cells were washed with PBS for three times. The fluorescence images of cells were observed by a fluorescence microscopy and the cells were measured by flow cytometry for quantitative analysis.

Cytotoxicity

To investigate the cell viability of free PTX, PTX-PTMs, and PTX-PSSTMs, HCT116, HT-29, and SW480 cells were seeded in 96-well plates and incubated for 24 h. After that, cells were treated with free PTX, PTX-PTMs, and PTX-PSSTMs containing PTX from 0.25 μ g/mL to 8 μ g/mL for 48 h. Cell viability was measured via MTT assay. Briefly, MTT (5 mg/mL, 10 μ L) was added to each well and incubated with cells for another 4 h. DMSO (100 μ L) was added to dissolve formazan crystals. The cell viability of blank mPEG_{1k}-TPE and mPEG_{1k}-SS-TPE micelles was determined by the same procedure. The absorbance (OD value) of each well was measured at 570 nm by a plate reader. Cell viability was calculated as follows:

$$\text{Cell viability}\% = \frac{\text{OD}_{\text{sample}} - \text{OD}_{\text{blank}}}{\text{OD}_{\text{control}} - \text{OD}_{\text{blank}}} \times 100\% \quad (3)$$

where OD_{sample} means the OD value from wells treated with drugs, OD_{control} from wells treated with growth medium, and OD_{blank} from wells without cells but culture medium.

To further demonstrate the influence of GSH on cytotoxicity of PTX-PSSTMs, cells were pre-treated with 10 mM GSH-OEt for 2 h. Then culture medium containing different PTX formulations (PTX 4 μ g/mL) was added and cells were incubated for 8 h. After that, culture medium with drugs was replaced with fresh medium without drugs and cells were incubated for another 40 h. At last, typical MTT assay was conducted to measure the cell viability.

Results and discussion

Synthesis of mPEG_{1k}-SS-TPE

The synthetic route of mPEG_{1k}-SS-TPE was depicted as shown in Scheme 2. Firstly, TPE-COOH was activated by DCC/NHS method to produce TPE-NHS (Fig. 1A). The signal peak b (δ 2.88) directly proved the successful activation. Then, TPE-SS-NH₂ was successfully synthesized by conjugating cystamine with TPE-NHS, which was proved by the disappearance of peak b and emergence of peak d, e, and c in Fig. 1B. To conjugate TPE-SS-NH₂ with mPEG, mPEG_{1k}-OH was modified with succinic anhydride to generate mPEG_{1k}-COOH that was characterized in Fig. 1C. Peak i (δ 2.64) was assigned to be methylene of succinic acid. At last, TPE-SS-NH₂ was reacted with activated mPEG_{1k}-COOH to generate mPEG_{1k}-SS-TPE. As shown in Fig. 1D, main signal peaks assigned to mPEG_{1k}-SS-TPE were listed, suggesting successful synthesis of mPEG_{1k}-SS-TPE. Specifically, the signal peak at δ 8.07 ppm was attributed to the generated amido bonds ($-\text{CONH}-$), which was the direct evidence demonstrating successful synthesis of mPEG_{1k}-SS-TPE compared with ¹H NMR spectrum of TPE-SS-NH₂ in Fig. 1B. mPEG_{1k}-TPE, without disulfide bonds, were successfully synthesized and characterized in Figure S1.

Characterization of micelles

The critical micelle concentration (CMC) is a key factor to demonstrate the stability of micelles for prolonged blood circulation. In this case, CMCs of mPEG_{1k}-SS-TPE and mPEG_{1k}-TPE were measured based on the AIE effect as the reports [25]. At the low concentration, polymers were in a free state in aqueous solution, and there was almost no fluorescence in the solution. However, when the concentration reached a critical value, the hydrophobic segments of polymers began to aggregate and the fluorescence of the solution increased significantly. As shown in Fig. 2A, CMCs of mPEG_{1k}-SS-TPE and mPEG_{1k}-TPE were measured to be 17.6 $\mu\text{g}/\text{mL}$ and 21.2 $\mu\text{g}/\text{mL}$, respectively. The CMC of mPEG_{1k}-SS-TPE was slightly smaller than that of mPEG_{1k}-TPE. To further evaluate the AIE effect, the fluorescence of mPEG_{1k}-SS-TPE in different H₂O/THF solution was detected as shown in Fig. 2B. With the increase of water content, mPEG_{1k}-SS-TPE aggregated gradually. When water fraction was up to 50%, significant fluorescence was visually observed.

Micelles based on mPEG_{1k}-SS-TPE were prepared by thin-film hydration method. The size distribution and morphology of mPEG_{1k}-SS-TPE micelles were investigated by DLS and TEM as shown in Fig. 2 C and D, respectively. DLS results revealed micelles with particle size of 95.2 ± 5.4 nm (PDI

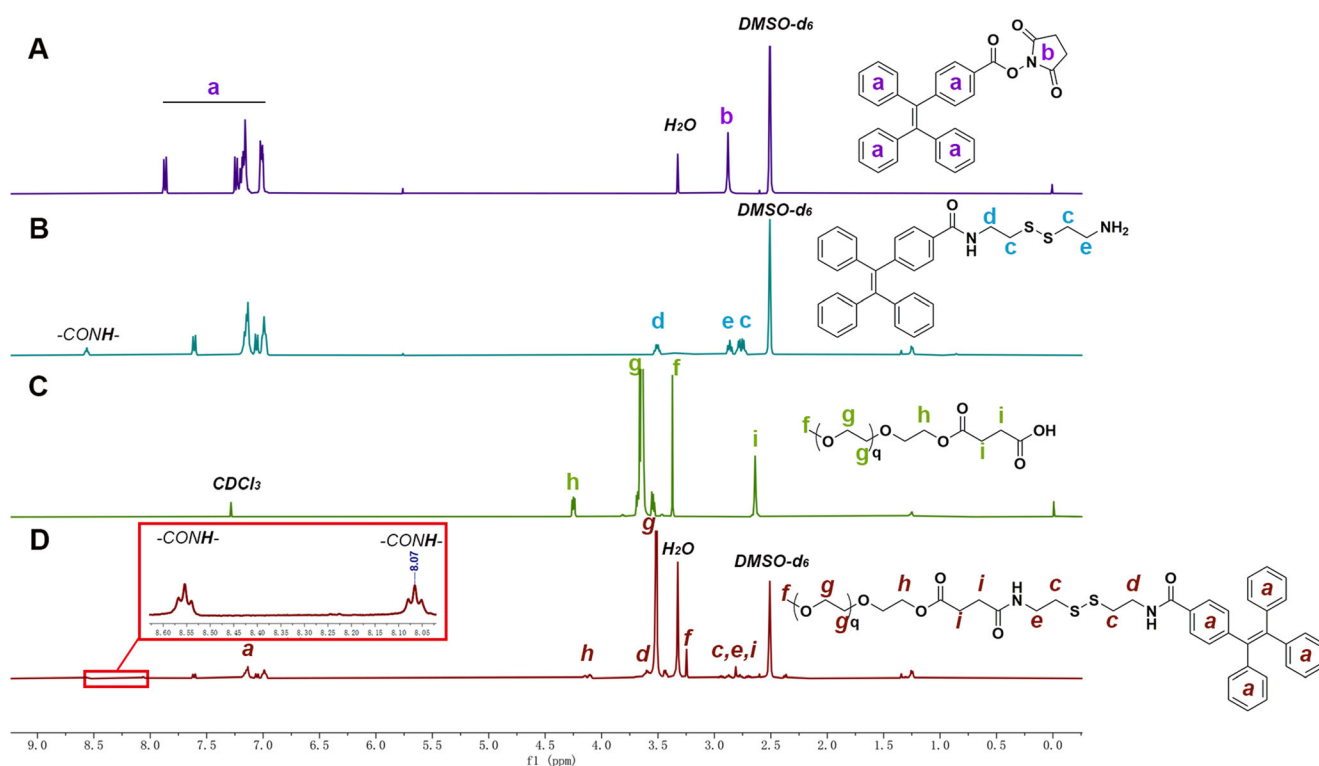


Fig. 1 ¹H NMR spectrum of TPE-NHS in DMSO-*d*₆ (A), TPE-SS-NH₂ in DMSO-*d*₆ (B), mPEG_{1k}-COOH in CDCl₃ (C), and mPEG_{1k}-SS-TPE in DMSO-*d*₆ (D)

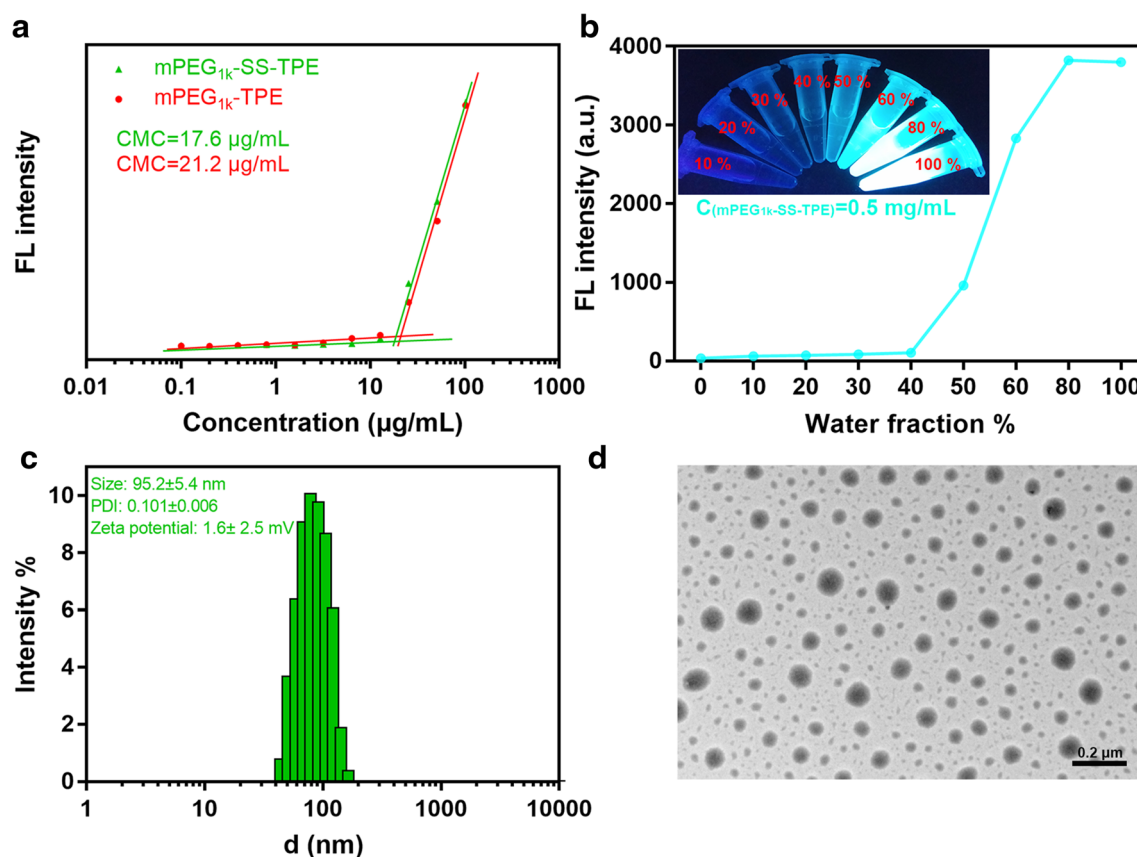


Fig. 2 CMCs of mPEG_{1k}-SS-TPE and mPEG_{1k}-TPE (A), fluorescent intensity and photos of mPEG_{1k}-SS-TPE in THF containing different amount of water (B), size distribution and Zeta potential of mPEG_{1k}-SS-TPE micelles (C), and morphology of mPEG_{1k}-SS-TPE micelles (D)

0.101 ± 0.006) with Zeta potential 1.6 ± 2.5 mV on average (Figure S2). And sphere appearance can be observed from TEM photos. The particle size observed by TEM was smaller than that measured by DLS, which is caused by the shrinkage of hydrophilic shell of micelles during preparation of TEM samples.

Reduction responsiveness

To characterize the reduction-responsive behavior, mPEG_{1k}-SS-TPE or mPEG_{1k}-TPE micelles were treated with 2 mM GSH and the scattering light intensity (SLI) was measured at predetermined time intervals. As shown in Fig. 3A, mPEG_{1k}-TPE micelles had relatively stable SLI values, while mPEG_{1k}-SS-TPE micelles exhibited gradually decreased SLI values, indicating disassembly of mPEG_{1k}-SS-TPE micelles. Figure 3B demonstrated changes of size distribution of mPEG_{1k}-SS-TPE micelles before and after 2 mM GSH treatment. Two signal peaks can be detected after GSH treatment, indicating degradation of mPEG_{1k}-SS-TPE micelles. Besides, TEM photo of mPEG_{1k}-SS-TPE micelles treated with GSH was taken as shown in Fig. 3C. Some aggregation was observed that was possibly formed by TPE residues. The fluorescent photos of mPEG_{1k}-SS-TPE or mPEG_{1k}-TPE micelles

treated with GSH were taken under irradiation at 365 nm as shown in Fig. 3D. After 6 h, no significant difference was observed by naked eyes. After 12 h, decreased fluorescence was observed in mPEG_{1k}-SS-TPE micelles. All these results suggested mPEG_{1k}-SS-TPE micelles can degrade at 2 mM GSH.

Drug encapsulation and release

PTX was encapsulated into mPEG_{1k}-SS-TPE micelles by thin-film hydration method. DLC and DLE of PTX-loaded mPEG_{1k}-SS-TPE micelles (PTX-PSSTMs) were measured to be 8.8% and 66.7%, respectively. PTX-PSSTMs exhibited sphere morphology with average size of 116 ± 3.9 nm in Fig. 4A, larger than blank mPEG_{1k}-SS-TPE micelles, which was possibly caused by drug loading to extend the hydrophobic core. To survey the influence of GSH concentrations on drug release, PTX-PSSTMs were incubated in PBS containing 20 µM, 2 mM, and 10 mM GSH. As reported, the concentration of GSH in the blood circulation and in extracellular matrices is approximately 2–20 µM, while 2–10 mM of GSH in intracellular space. As shown in Fig. 4B, PTX-PSSTMs exhibited slower PTX release in PBS with 20 µM GSH than that with 2 mM GSH. When

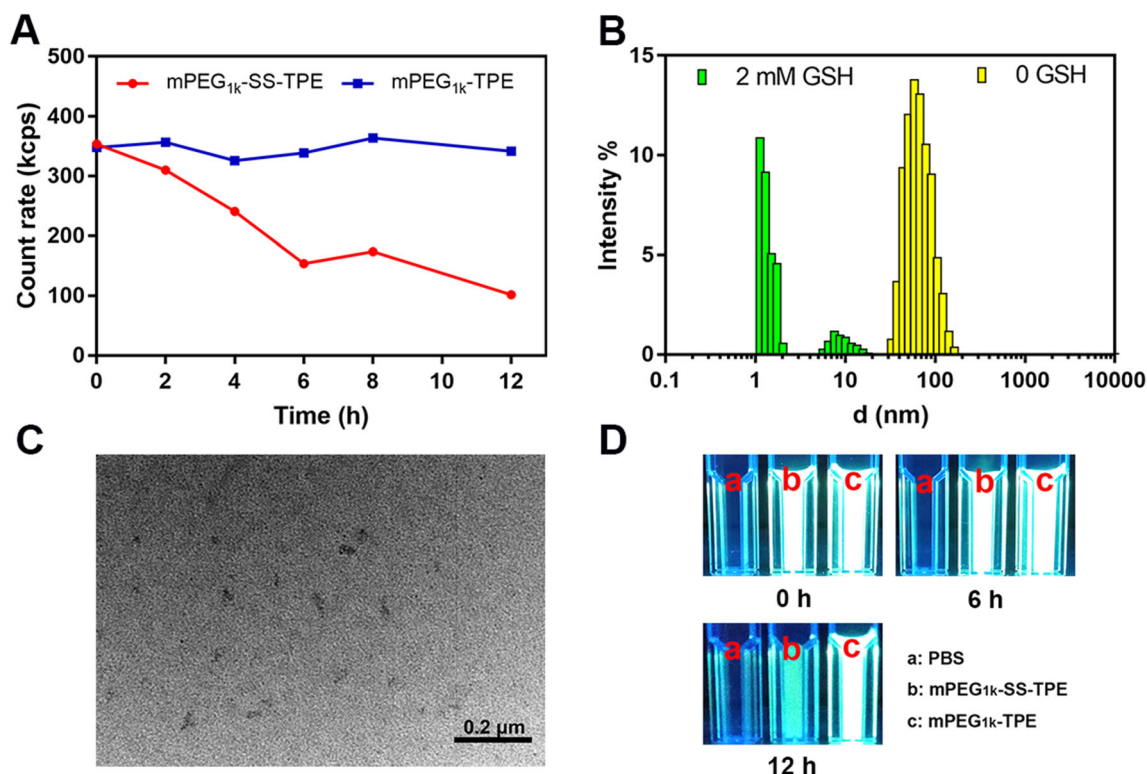


Fig. 3 Scattering light intensity of mPEG_{1k}-SS-TPE or mPEG_{1k}-TPE micelles with 2 mM GSH at different time intervals (A), size distribution of mPEG_{1k}-SS-TPE micelles before and after GSH

treatment (B), TEM photo of mPEG_{1k}-SS-TPE micelles after GSH treatment (C), and fluorescence photos of mPEG_{1k}-SS-TPE or mPEG_{1k}-TPE micelles under irradiation at 365 nm (D)

PTX-PSSTMs were incubated in PBS with 10 mM GSH, drug release was further accelerated. Specifically, cumulative release for 40 h was 19.1% in 20 μM GSH condition, while 53.1% in 2 mM GSH condition and 75.2% in 10 mM GSH condition. However, as a comparison, when PTX release from PTX-loaded mPEG_{1k}-TPE micelles (PTX-PTMs) was simulated in PBS containing 10 mM, the release profile was similar to that of PTX-PSSTMs in 20 μM GSH condition. These results indicated that PTX release was triggered by high level of GSH and exhibited a GSH-dependent behavior.

Cellular uptake

To evaluate the intracellular uptake, SW480 were treated with Nile Red-loaded mPEG_{1k}-TPE or mPEG_{1k}-SS-TPE micelles. As shown in Fig. 5, blue fluorescence of AIE micelles was easily identified. Cells exhibited obvious blue fluorescence after 1-h incubation with mPEG_{1k}-SS-TPE micelles, while weak blue fluorescence was observed after 0.5-h incubation, indicating more mPEG_{1k}-SS-TPE micelles internalized into cells. Interestingly, blue fluorescence was significantly decreased after 2-h incubation

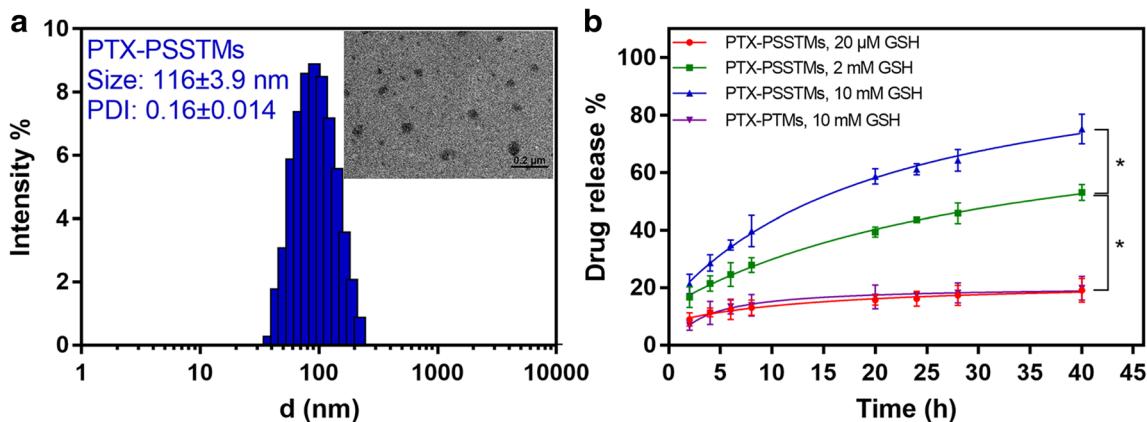


Fig. 4 Size distribution and morphology of PTX-PSSTMs (A) and PTX release profiles from PTX-PSSTMs in PBS containing 20 μM, 2 mM and 10 mM GSH (B). Asterisk represents $p < 0.05$

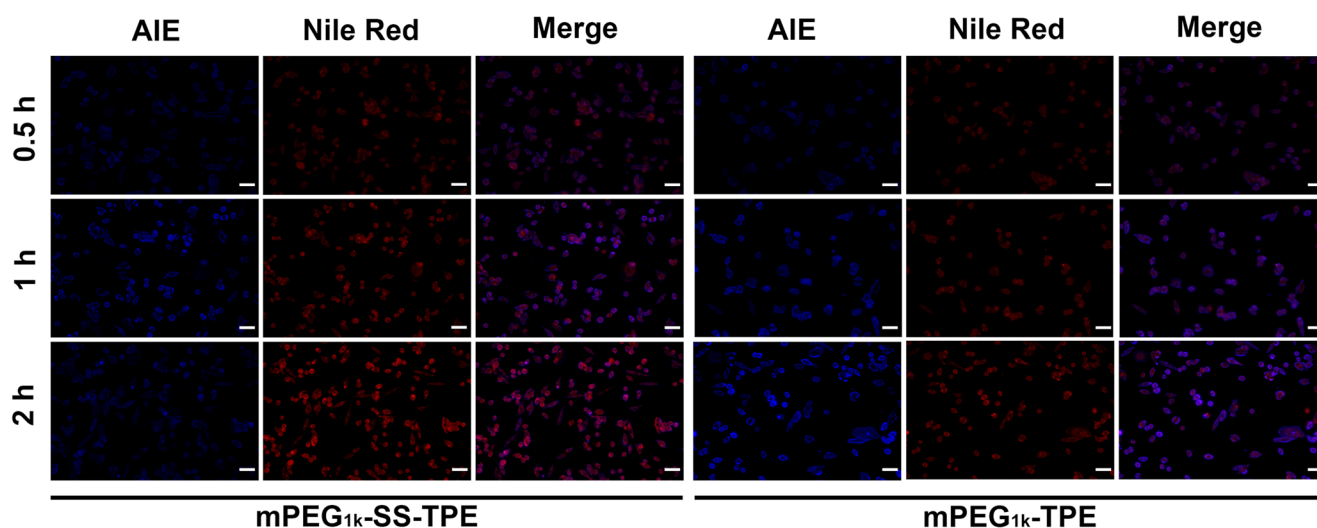
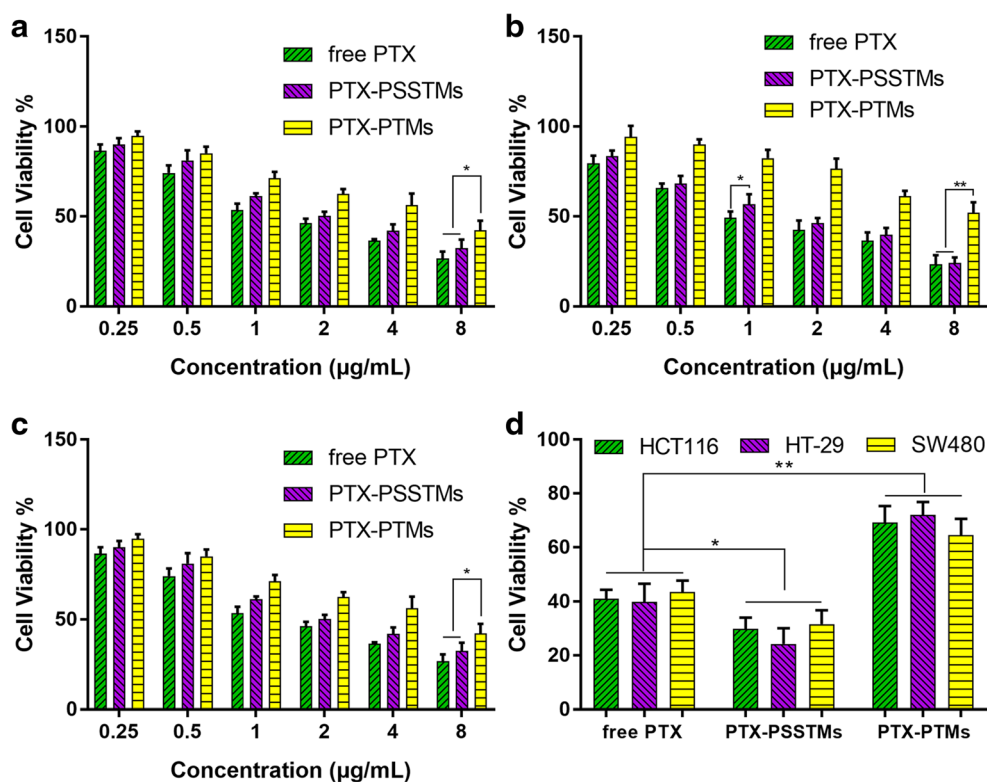


Fig. 5 Fluorescence images of SW480 cells exposed to Nile Red–loaded mPEG_{1k}-SS-TPE or mPEG_{1k}-TPE micelles. Scale bar, 50 μ m

compared with 1-h incubation. Besides, it was worth noting that red fluorescence of Nile Red was gradually increased during 2-h incubation. However, when cells were treated with Nile Red–loaded mPEG_{1k}-TPE micelles for 0.5 h, 1 h, and 2 h, cells exhibited increased blue fluorescence but the increase of red fluorescence was not obvious compared with that of Nile Red–loaded mPEG_{1k}-SS-TPE micelles. The quantitative analysis of cellular uptake by flow cytometry was shown in Figure S3. Red fluorescence of cells treated with both Nile Red–loaded micelles

increased gradually over time. It was noteworthy that red fluorescence intensity resulted from Red-loaded mPEG_{1k}-SS-TPE micelles was higher than that from Red-loaded mPEG_{1k}-TPE micelles, especially for 1 h and 2 h. These results were probably caused by the degradation of mPEG_{1k}-SS-TPE micelles, and increased red fluorescence can be explained by two main reasons: (1) more micelles entered the tumor cells by prolonging the culture time; (2) Nile Red was released from micelles and the ACQ effect of Nile Red weakened with the degradation of micelles.

Fig. 6 Cytotoxicity of free PTX, PTX-PSSTMs, and PTX-PTMs against HCT116 cells (A), HT-29 cells (B), and SW480 cells (C); cell viability of free PTX, PTX-PSSTMs, and PTX-PTMs (PTX 4 μ g/mL) against HCT116, HT-29, and SW480 cells pretreated with GSH-OEt (D). Single asterisk represents $p < 0.05$ and double asterisk represent $p < 0.01$



Cytotoxicity

The cytotoxicity of blank mPEG_{1k}-TPE or mPEG_{1k}-SS-TPE micelles was evaluated against HCT116, HT-29, and SW480 cells as shown in Figure S4. Both mPEG_{1k}-TPE and mPEG_{1k}-SS-TPE micelles exhibited almost no cytotoxicity at all tested concentrations, indicating great biocompatibility. The cell viability of HCT116, HT-29, and SW480 cells treated with free PTX, PTX-PSSTMs, and PTX-PTMs was demonstrated in Fig. 6. Both free PTX and PTX-PSSTMs exhibited comparable cytotoxicity against HCT116 cells with the half maximal inhibitory concentration (IC₅₀) of 0.56 μg/mL and 0.55 μg/mL, respectively, as shown in Table 1. However, free PTX exhibited slightly higher cytotoxicity against HT-29 and SW480 cells in comparison with PTX-PSSTMs. It was worth noting that IC₅₀ values of PTX-PTMs were significantly lower than that of free PTX and PTX-PSSTMs on all tested cells. Specifically, IC₅₀ value of PTX-PTMs against HT-29 was more than six times that of free PTX and three times that of PTX-PSSTMs. As reported, GSH-OEt was often used to artificially improve the intracellular GSH concentrations [31]. When cells were pre-treated with GSH-OEt to increase the amount of GSH in tumor cells, PTX-PSSTMs exhibited higher cell inhibition than free PTX against all tested cells as shown in Fig. 6D, while PTX-PTMs still exhibited lower cell inhibition than free PTX. All these results indicated that PTX release from PTX-PSSTMs was controlled by GSH, which was in accordance with the results of Fig. 4B.

Conclusion

In conclusion, amphiphilic polymers, mPEG_{1k}-SS-TPE, were synthesized and can self-assemble into nanomicelles in water. mPEG_{1k}-SS-TPE micelles showed narrow size distribution and sphere morphology. After being loaded with PTX, PTX-PSSTMs exhibited reduction-sensitive drug release profiles compared with PTX-PTMs. Visually, cellular uptake experiments demonstrated efficient Nile Red delivery and self-located AIE imaging. In addition, mPEG_{1k}-SS-TPE micelles exhibited decreased AIE fluorescence compared with

Table 1 IC₅₀ values of different PTX formulation against HCT116, HT-29, and SW480 cells

	IC ₅₀ /μg/mL		
	HCT116	HT-29	SW480
Free PTX	0.56	0.60	0.65
PTX-PTMs	1.17	3.69	1.13
PTX-PSSTMs	0.55	0.99	0.80

mPEG_{1k}-TPE micelles, indicating degradation of mPEG_{1k}-SS-TPE micelles. PTX-PSSTMs exhibited higher cytotoxicity against SW480, HCT116, and HT-29 than PTX-PTMs. After cells were treated with GSH-OEt, PTX-PSSTMs exhibited higher cytotoxicity than free PTX.

Compliance with ethical standards

Conflict of interest The authors declare that they have no conflict of interest.

References

- Li J, Wang J, Zhang X, Xia X, Zhang C (2019) Biodegradable reduction-responsive polymeric micelles for enhanced delivery of melphalan to retinoblastoma cells. *Int J Biol Macromol* 141:997–1003. <https://doi.org/10.1016/j.jbiomac.2019.09.085>
- Trubitsyn G, Nguyen VN, Di Tommaso C et al (2019) Impact of covalently Nile Red and covalently Rhodamine labeled fluorescent polymer micelles for the improved imaging of the respective drug delivery system. *Eur J Pharm Biopharm* 142:480–487. <https://doi.org/10.1016/j.ejpb.2019.07.020>
- Wang C, Zhu J, Ma J, Yang Y, Cui X (2019) Functionalized Bletilla striata polysaccharide micelles for targeted intracellular delivery of Doxorubicin: In vitro and in vivo evaluation. *Int J Pharm* 567:118436. <https://doi.org/10.1016/j.ijpharm.2019.06.027>
- Jiang M, Zhang E, Liang Z, Zhao Y, Zhang S, Xu H, Wang H, Shu X, Kang X, Sun L, Zhen Y (2019) Liposome-based co-delivery of 7-O-geranyl-quercetin and IGF-1R siRNA for the synergistic treatment of non-small cell lung cancer. *J Drug Deliv Sci Technol* 54: 101316. <https://doi.org/10.1016/j.jddst.2019.101316>
- Katayama T, Kinugawa S, Takada S, Furihata T, Fukushima A, Yokota T, Anzai T, Hibino M, Harashima H, Yamada Y (2019) A mitochondrial delivery system using liposome-based nanocarriers that target myoblast cells. *Mitochondrion* 49:66–72. <https://doi.org/10.1016/j.mito.2019.07.005>
- Xiao Y, Liu Q, Clulow AJ, Li T, Manohar M, Gilbert EP, de Campo L, Hawley A, Boyd BJ (2019) PEGylation and surface functionalization of liposomes containing drug nanocrystals for cell-targeted delivery. *Colloids Surfaces B Biointerfaces* 182: 110362. <https://doi.org/10.1016/j.colsurfb.2019.110362>
- Mukherjee S, Kotcherlakota R, Haque S, Bhattacharya D, Kumar JM, Chakravarty S, Patra CR (2020) Improved delivery of doxorubicin using rationally designed PEGylated platinum nanoparticles for the treatment of melanoma. *Mater Sci Eng C* 108:110375. <https://doi.org/10.1016/j.msec.2019.110375>
- Wang S, Chen Y, Wang S, Li P, Mirkin CA, Farha OK (2019) DNA-functionalized metal-organic framework nanoparticles for intracellular delivery of proteins. *J Am Chem Soc* 141:2215–2219. <https://doi.org/10.1021/jacs.8b12705>
- Qiu L, Zhao L, Xing C, Zhan Y (2018) Redox-responsive polymer prodrug/AgNPs hybrid nanoparticles for drug delivery. *Chinese Chem Lett* 29:301–304. <https://doi.org/10.1016/j.ccl.2017.09.048>
- Hung WH, Zheng JH, Lee KC, Cho EC (2019) Doxorubicin conjugated AuNP/biopolymer composites facilitate cell cycle regulation and exhibit superior tumor suppression potential in KRAS mutant colorectal cancer. *J Biotechnol* 306:149–158. <https://doi.org/10.1016/j.jbiotec.2019.09.015>
- Park J, Choi Y, Chang H, Um W, Ryu JH, Kwon IC (2019) Alliance with EPR effect: combined strategies to improve the EPR effect in the tumor microenvironment. *Theranostics* 9:8073–8090. <https://doi.org/10.7150/thno.37198>

12. Yoshikawa T, Mori Y, Feng H, Phan KQ, Kishimura A, Kang JH, Mori T, Katayama Y (2019) Rapid and continuous accumulation of nitric oxide-releasing liposomes in tumors to augment the enhanced permeability and retention (EPR) effect. *Int J Pharm* 565:481–487. <https://doi.org/10.1016/j.ijpharm.2019.05.043>
13. Kalyane D, Raval N, Maheshwari R, Tambe V, Kalia K, Tekade RK (2019) Employment of enhanced permeability and retention effect (EPR): nanoparticle-based precision tools for targeting of therapeutic and diagnostic agent in cancer. *Mater Sci Eng C* 98: 1252–1276. <https://doi.org/10.1016/j.msec.2019.01.066>
14. Yang M, Ding H, Zhu Y, Ge Y, Li L (2019) Co-delivery of paclitaxel and doxorubicin using mixed micelles based on the redox sensitive prodrugs. *Colloids Surfaces B Biointerfaces* 175:126–135. <https://doi.org/10.1016/j.colsurfb.2018.11.086>
15. Du J, Choi B, Liu Y et al (2019) Degradable pH and redox dual responsive nanoparticles for efficient covalent drug delivery. *Polym Chem* 10:1291–1298. <https://doi.org/10.1039/c8py01583j>
16. Dhawan S, Ghosh S, Ravinder R, Bais SS, Basak S, Krishnan NMA, Agarwal M, Banerjee M, Haridas V (2019) Redox sensitive self-assembling dipeptide for sustained intracellular drug delivery. *Bioconjug Chem* 30:2458–2468. <https://doi.org/10.1021/acs.bioconjchem.9b00532>
17. Xiang Y, Duan X, Feng L, Jiang S, Deng L, Shen J, Yang Y, Guo R (2019) tLyp-1-conjugated GSH-sensitive biodegradable micelles mediate enhanced pUNO1-hTRAILa/curcumin co-delivery to gliomas. *Chem Eng J* 374:392–404. <https://doi.org/10.1016/j.cej.2019.05.186>
18. Sun J, Liu Y, Chen Y, Zhao W, Zhai Q, Rathod S, Huang Y, Tang S, Kwon YT, Fernandez C, Venkataraman R, Li S (2017) Doxorubicin delivered by a redox-responsive dasatinib-containing polymeric prodrug carrier for combination therapy. *J Control Release* 258:43–55. <https://doi.org/10.1016/j.jconrel.2017.05.006>
19. Qu Y, Chu B, Wei X, Lei M, Hu D, Zha R, Zhong L, Wang M, Wang F, Qian Z (2019) Redox/pH dual-stimuli responsive camptothecin prodrug nanogels for “on-demand” drug delivery. *J Control Release* 296:93–106. <https://doi.org/10.1016/j.jconrel.2019.01.016>
20. Youmei L, Qian W, Miaomiao K et al (2020) Boosting the photodynamic therapy efficiency by using stimuli-responsive and AIE-featured nanoparticles. *Biomaterials* 232:119749. <https://doi.org/10.1016/j.biomaterials.2019.119749>
21. Wang D, Lee MMS, Xu W, Kwok RTK, Lam JWY, Tang BZ (2018) Theranostics based on AIEgens. *Theranostics* 8:4925–4956. <https://doi.org/10.7150/thno.27787>
22. Dai YD, Sun XY, Sun W, Yang JB, Liu R, Luo Y, Zhang T, Tian Y, Lu ZL, He L (2019) H₂O₂-responsive polymeric micelles with a benzil moiety for efficient DOX delivery and AIE imaging. *Org Biomol Chem* 17:5570–5577. <https://doi.org/10.1039/c9ob00859d>
23. Yu T, Zhuang W, Su X, Ma B, Hu J, He H, Li G, Wang Y (2019) Dual-responsive micelles with aggregation-induced emission feature and two-photon absorption for accurate drug delivery and bioimaging. *Bioconjug Chem* 30:2075–2087. <https://doi.org/10.1021/acs.bioconjchem.9b00364>
24. Dong Z, Bi Y, Cui H, Wang Y, Wang C, Li Y, Jin H, Wang C (2019) AIE supramolecular assembly with FRET effect for visualizing drug delivery. *ACS Appl Mater Interfaces* 11:23840–23847. <https://doi.org/10.1021/acsami.9b04938>
25. Zhang C, Jin S, Yang K, Xue X, Li Z, Jiang Y, Chen WQ, Dai L, Zou G, Liang XJ (2014) Cell membrane tracker based on restriction of intramolecular rotation. *ACS Appl Mater Interfaces* 6:8971–8975. <https://doi.org/10.1021/am5025897>
26. He X, Yin F, Wang D, Xiong LH, Kwok RTK, Gao PF, Zhao Z, Lam JWY, Yong KT, Li Z, Tang BZ (2019) AIE featured inorganic-organic core@shell nanoparticles for high-efficiency siRNA delivery and real-time monitoring. *Nano Lett* 19:2272–2279. <https://doi.org/10.1021/acs.nanolett.8b04677>
27. Chen Y, Han H, Tong H, Chen T, Wang H, Ji J, Jin Q (2016) Zwitterionic phosphorylcholine-TPE conjugate for pH-responsive drug delivery and AIE active imaging. *ACS Appl Mater Interfaces* 8:21185–21192. <https://doi.org/10.1021/acsami.6b06071>
28. Gao Y, Wei K, Li J, Li Y, Hu J (2018) A facile four-armed AIE fluorescent sensor for heparin and protamine. *Sensors Actuators, B Chem* 277:408–414. <https://doi.org/10.1016/j.snb.2018.09.054>
29. Feng X, Zhou Y, Xie X, Li M, Huang H, Wang L, Xu X, Yu J (2019) Development of PSMA-targeted and core-crosslinked glycol chitosan micelles for docetaxel delivery in prostate cancer therapy. *Mater Sci Eng C* 96:436–445. <https://doi.org/10.1016/j.msec.2018.11.044>
30. Li Y, Xiao W, Xiao K, Berti L, Luo J, Tseng HP, Fung G, Lam KS (2012) Well-defined, reversible boronate crosslinked nanocarriers for targeted drug delivery in response to acidic pH values and cis-diols. *Angew Chemie - Int Ed* 51:2864–2869. <https://doi.org/10.1002/anie.201107144>
31. Sun H, Meng F, Cheng R, Deng C, Zhong Z (2013) Reduction-sensitive degradable micellar nanoparticles as smart and intuitive delivery systems for cancer chemotherapy. *Expert Opin Drug Deliv* 10:1109–1122. <https://doi.org/10.1517/17425247.2013.783009>

Publisher's note Springer Nature remains neutral with regard to jurisdictional claims in published maps and institutional affiliations.